



Solar-Fenton removal of malachite green with novel Fe⁰-activated carbon nanocomposite

Pardeep Singh ^{a,*}, Pankaj Raizada ^a, Shailza Kumari ^a, Amit Kumar ^a, Deepak Pathania ^a, Pankaj Thakur ^{a,b}

^a School of Chemistry, Faculty of Basic Science, Shoolini University, Solan Himachal Pradesh, 173212, India

^b Center for Advanced Biomaterials for Health Care (Istituto Italiano Di Tecnologia) Largo Barsanti e Matteucci 53, 80125 Naples, Italy



ARTICLE INFO

Article history:

Received 4 October 2013

Received in revised form

10 December 2013

Accepted 8 February 2014

Available online 17 February 2014

Keywords:

Fe⁰-AC

Solar-Fenton reaction

Oxidative removal

Recycle efficiency

ABSTRACT

Zero valent iron-activated carbon nanocomposite (Fe⁰-AC) was synthesized using liquid phase reduction method. Both Fe⁰-AC and micro zero valent iron (ZVI) were characterized by scanning electron microscope (SEM), transmission electron microscopy (TEM), X-ray Diffraction (XRD), Fourier Transform Infrared (FTIR), UV-visible (UV-vis) spectral techniques. The size of Fe⁰-AC was observed to be 50 nm. The catalytic efficiency of Fe⁰-AC was explored for the removal of malachite green dye (MG) from aqueous phase. Fe⁰-AC induced solar-Fenton removal of MG was investigated in the presence of H₂O₂ and citrate (cit.). Solar/H₂O₂/cit./Fe⁰-AC system exhibited highest removal efficiency among investigated photocatalytic systems. The dye removal was strongly influenced by solar light, pH, Fe⁰-AC dosage, H₂O₂ and citrate concentration in reaction system. The reaction was maximal at pH 6.75. MG was completely decolorized in 60 min using solar/H₂O₂/cit./Fe⁰-AC system. Hydroxyl radicals (OH[•]) were the main oxidizing species during solar-Fenton process.

Fe⁰-AC proved to be a potential adsorbent for MG. Fe⁰-AC showed high recycle efficiency due to easier separation from aqueous phase. The lower concentration of dissolved Fe(II) ions in reaction solution indicated the stability of Fe⁰-AC during MG removal. On the basis of obtained results, the most plausible mechanism for oxidative removal MG of was proposed.

© 2014 Elsevier B.V. All rights reserved.

1. Introduction

Advanced oxidation processes (AOPs) have gained immense importance owing to their applicability in wastewater treatment in recent years. Habitually, AOPs are characterized by the formation of highly reactive species (H₂O₂, OH[•], O₂[−], OH²[−]) to degrade refractory organic/inorganic compounds present in wastewater [1,2]. Among AOPs based remediation technology, homogenous Fenton reactions have emerged as important way to generate highly reactive and non-selective OH[•] radicals [3,4]. The generated OH[•] radicals have high oxidizing ability and degrade persistent and non-biodegradable pollutants present in aquatic environment [5]. The efficiency of Fenton process can be improved by the use of visible light [6]. Moreover, heterogeneous photo-Fenton reactions have attracted many researchers due to high reaction efficiency and easier separation of photocatalyst from treated water [7].

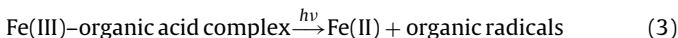
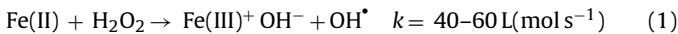
Several heterogeneous photocatalysts such as Fe₂O₃ hollow sphere [8], Cu modified iron oxide [9], silica supported iron oxide [10], Fe⁰-supported on resins [11] and pillared clays [12] have been prepared for wastewater treatment.

For the past fifteen years, ZVI particles have been widely used to reduce various contaminants present in wastewater [13]. Nano-zero valent iron (nZVI) exhibits at least 25–30 times faster reactivity than bulk ZVI [14]. nZVI is highly effective for the degradation of β-lactam antibiotics (amoxicillin and ampicillin) [15], metronidazole antibiotic [16], azo dyes [17], chlorinated solvents [18], chlorinated pesticides [19], organophosphates [20], nitroaromatics [21] and p-chlorophenol [22]. However, degradation rate is retarded by very limited mobility of nZVI due to particle aggregation [23]. In order to overcome these drawbacks, recent studies have been focused on the incorporation of ZVI with different organic/inorganic supports. Xu et al. prepared nanoscale iron hydroxide doped granular activated carbon for the adsorption of perchlorate in water [24]. Commercial activated carbon (CAC) seems to be an excellent supporting material for nZVI because of its high chemical stability, mechanical robustness, large specific surface area and commercial availability [25].

* Corresponding author. Tel.: +91 1792 308000; fax: +91 1792 30800.

E-mail addresses: pardeepchem@gmail.com (P. Singh), pankajchem1@gmail.com (P. Raizada).

Most of ZVI based remediation techniques are reductive in nature [26]. However, in the presence of $\text{H}_2\text{O}_2/\text{ZVI}$, hydroxyl radicals are generated through Fenton reaction leading to the oxidation of organic compounds. The consecutive formation of Fe(II) is needed to maintain the efficiency of Fenton process. However, the rate of Fe(II) formation is comparatively low in H_2O_2 and ZVI mediated Fenton reaction (Eqs. (1) and (2)).



The combination of visible light and organic acid enhances the regeneration of Fe(II) through photo-transformation of Fe(III)-organic acid complex into Fe(II) and organic radicals(Eq. (3)) as well as resulting into additional OH^\bullet radical formation [27]. At the same, organic acid can be used as pH buffer to maintain constant pH of reaction system [28]. Katsumata et al. introduced UV/Fe(II)-citrate/ H_2O_2 system at pH 8.0 for alachlor degradation [29]. Silva et al. investigated degradation of herbicide tebuthiuron using UV-Fenton and ferric citrate complex system at neutral pH [30]. Lucas and Peres explored UV/Fenton and ferrioxalate/ H_2O_2 /solar light based processes with dissolved iron to degrade reactive black dye [31].

In precedent work, we preferred the use of $\text{Fe}^0\text{-AC}$ instead of nZVI powder to reduce the difficulties in separating ZVI particles. Solar light was used throughout the experiment rather than expensive artificial source of light. The foremost objective of our research was to explore the photocatalytic efficiency of solar/ $\text{H}_2\text{O}_2/\text{cit}/\text{Fe}^0\text{-AC}$ system for MG degradation in aqueous medium. The effect of reaction parameters such as $\text{Fe}^0\text{-AC}$ dosage, pH, citrate and H_2O_2 concentration on MG removal was also investigated. The adsorption behavior of $\text{Fe}^0\text{-AC}$ was also explored for the MG removal.

2. Materials and methods

2.1. Chemicals

All the chemicals used in this study were of analytical grade. Ferrous sulphate ($\text{FeSO}_4 \cdot 7\text{H}_2\text{O}$) and powdered activated carbon (200 mesh) were purchased from Sigma-Aldrich, India. Polyethylene glycol 6000 (PEG 6000), hydrogen peroxide, ethanol, hydrochloric acid (HCl), sodium borohydride (NaBH_4), malachite green, 1,10-phenanthroline monohydrate, isopropanol and sodium citrate ($\text{Na}_3\text{C}_6\text{H}_5\text{O}_7$) were obtained from Merck, India. All the solutions were prepared in doubly distilled water.

2.2. Synthesis of $\text{Fe}^0\text{-AC}$

The synthesis of $\text{Fe}^0\text{-AC}$ was performed using liquid phase reduction method [32]. In typical synthesis, powdered activated carbon was washed with distilled water and dried at 60 °C overnight. In the next step, 1.5 g of $\text{FeSO}_4 \cdot 7\text{H}_2\text{O}$ and 1.2 g of dried activated carbon were mixed in 100 mL distilled water and heated at 50 °C for 20 min. To this mixture, 70% ethanol (100 mL) and 1.0 g of polyethylene glycol 6000 (PEG 6000) were added with constant stirring. The reaction pH was adjusted to 7.5 using 1 M NaOH. In the next step, 0.5 M sodium borohydride (NaBH_4) was added dropwise with constant stirring for 3 h to obtain black colored precipitates. The precipitates were filtered and washed with degassed water and finally vacuum dried. The obtained product was leveled as $\text{Fe}^0\text{-AC}$ and placed in anaerobic chamber filled with pure N_2 gas prior to use. This methodology was also adopted for the preparation of ZVI with no addition of activated carbon powder.

2.3. Adsorption and photocatalytic experiments

Double walled pyrex vessel (ht. 7.5 cm × dia. 6 cm) was used to investigate adsorptional and photocatalytic activity of $\text{Fe}^0\text{-AC}$. The pyrex vessel was surrounded by thermostatic water circulation arrangement to keep temperature in the range of 30 ± 0.3 °C (Fig. 1). During adsorption experiments, slurry composed of dye solution and catalyst suspension was stirred magnetically and placed in

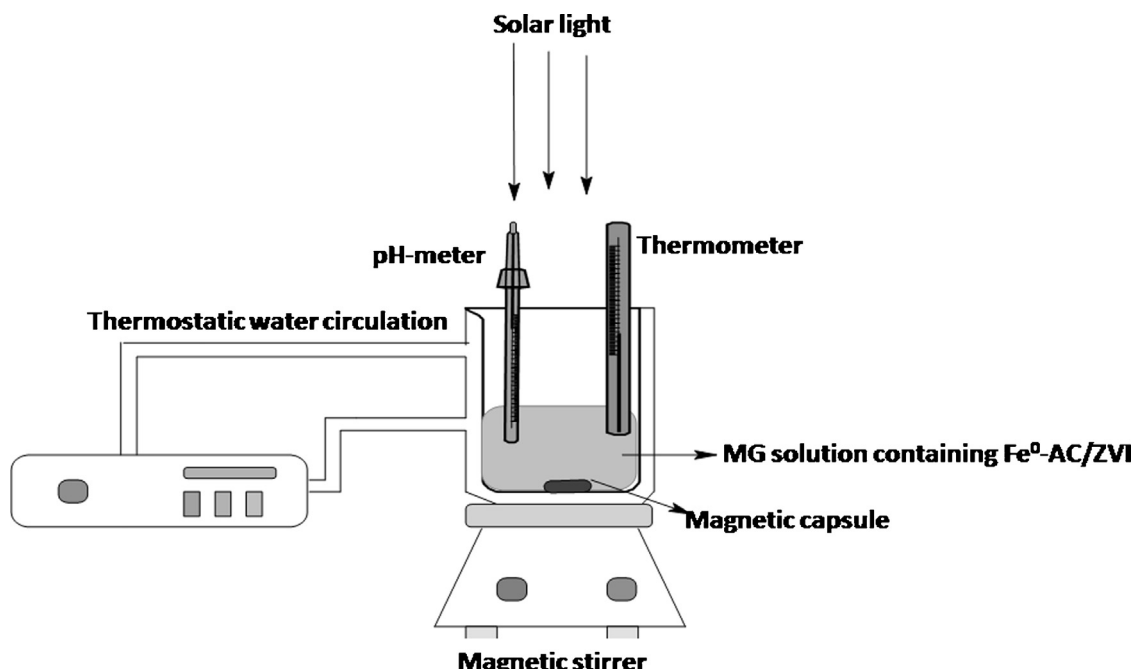


Fig. 1. Schematic diagram of photoreactor.

dark to equilibrate adsorption and desorption of MG molecule onto catalyst surface. Prior to photocatalytic studies, suspension composed of dye and catalyst was stirred for ten min in dark. Then suspension was exposed to solar light with continuous stirring. At specific time intervals, aliquot (3 mL) was withdrawn and centrifuged for 2 min to remove catalyst particles from aliquot. The concentration of MG in supernatant was determined on double-beam UV-Vis spectrophotometer at 620 nm. The average intensity of solar light between 11 am to 2 pm was measured by a digital lux-meter ($35 \times 10^3 \pm 1000$ lx). All the photocatalytic experiments were performed in March to May 2012 between 11 am to 2 pm. All the experiments were undertaken in triplicate with errors below 5% and average values were reported. The removal efficiency was calculated using following equation:

$$\% \text{removal efficiency} = \frac{C_0 - C_t}{C_0} \times 100 \quad (4)$$

where C_0 is the initial concentration and C_t is instant concentration of dye sample. Fe(II) concentration was determined spectrophotometrically (absorbance measurement at 510 nm) by 1,10-phenanthroline method [33]. The kinetics of MG degradation was explained by pseudo first order kinetics. The rate constant (k) were calculated using Eq. (5):

$$k = 2.303 \times \text{slope} \quad (5)$$

where the slope was obtained from the plot of $\ln(\text{absorbance})$ versus t .

2.4. Determination of pH of zero point charge

The pH of zero point charge (pH_{ZPC}) was estimated by pH drift method [34]. For this purpose, 50 mL solutions of 0.01 M sodium chloride were adjusted to initial pH values between 2 and 12 in. Then, AC/Fe⁰-AC (0.10 g) was added into this solution. After 48 h, final pH of solution was measured and plotted against initial pH. The pH at which the curve crossed the line of equality was taken as the pH_{ZPC} of AC and Fe⁰-AC.

2.5. Characterization of Fe⁰-AC

SEM micrographs have been obtained through a Quant-250, model 9393 by attaching the powder samples onto adhesive carbon tapes supported on metallic disks. Sample surfaces were then observed at different magnifications and images were recorded. Energy dispersive X-ray (EDX) analysis was performed at randomly selected locations on the solid surfaces. EDX mapping was carried out at 1000 \times magnification under vacuum conditions. The microstructure of Fe⁰-AC was analyzed using TEM (Tecnai 20 G2 Plate/CCD Camera). Fourier-transform Infrared Spectra (FTIR) was obtained using Perkin Elmer spectrometer (Spectrum 400, USA). XPERT-PRO diffractometer system was used for powder XRD analysis. UV-visible analysis was performed using UV-Visible spectrophotometer (Systronics 117). Cu K α radiations at wavelength of 1.54 Å were used as the source of X-rays. Fe⁰-AC particles were placed in glass holder and were recorded over 2 θ range of 10°–100°. Crystalline size of Fe⁰-AC was calculated using Debye-Scherer formula (Eq. (6)):

$$D = \frac{k\lambda}{\beta \cos\theta} \quad (6)$$

where D =the thickness of the nanocrystal, k (constant)=(0.9), λ =wavelength of X-rays (1.54 Å), β =width at half maxima of reflection at Bragg's angle 2θ (θ =Bragg's angle).

3. Results and discussion

3.1. Characterization of Fe⁰-AC, AC and ZVI

3.1.1. SEM, TEM, EDX, XRD and UV-vis analysis of AC, Fe⁰-AC and ZVI

Fig. 2 a and b depicts the uniform porous nature of activated carbon. These pores (10 µm) provided a good possibility for ZVI particles to be trapped inside them. **Fig. 2c and d** indicates that in the absence of activated carbon, ZVI particles were found to agglomerate more rapidly to microsphere of 20 µm. **Fig. 2e and f** confirms the presence of both zero valent iron and activated carbon in Fe⁰-AC. Fe⁰ aggregates were uniformly dispersed over activated carbon matrix.

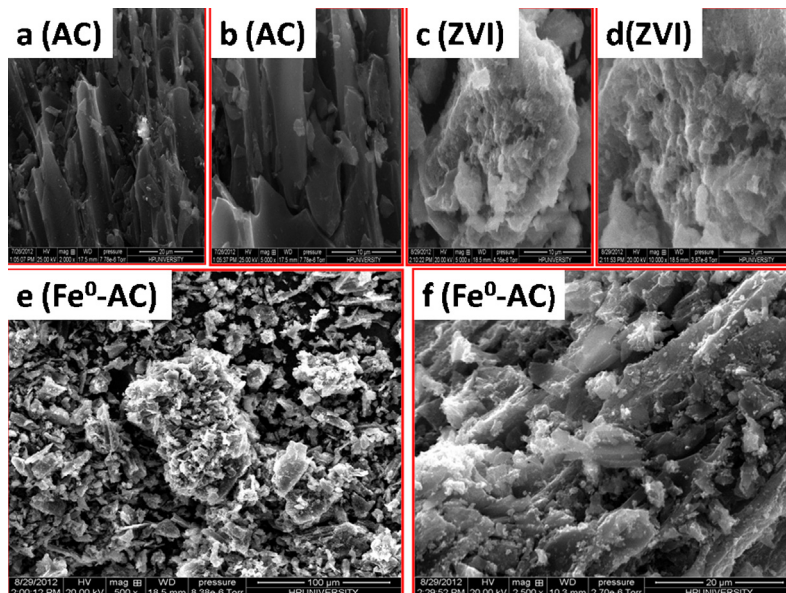


Fig. 2. (a-f) SEM images of activated carbon (a and b), zero valent iron (c and d) and Fe⁰-AC (e and f) at 2000 (a), 5000 (b), 5000 (c), 10,000 (d), 500 (e) and 5000 (d) magnifications.

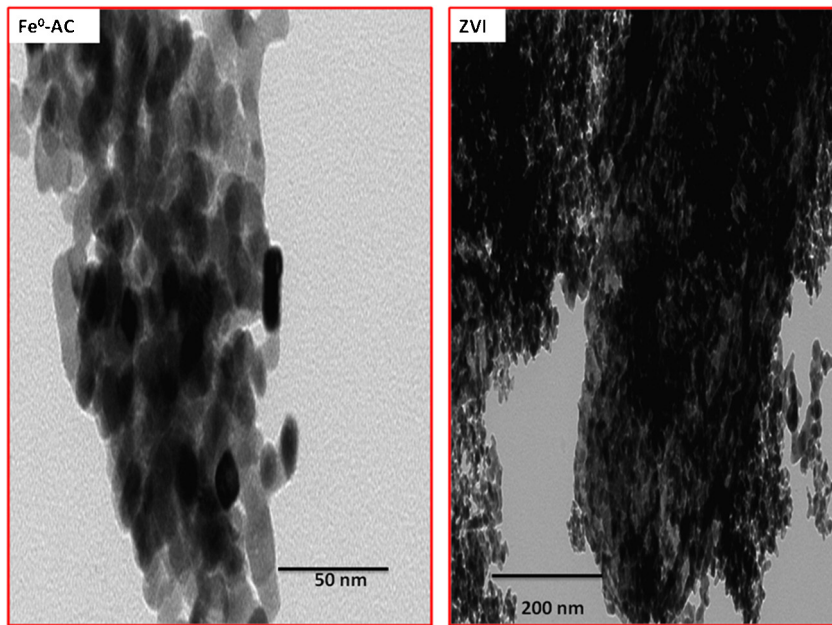


Fig. 3. TEM images of Fe⁰-AC and zero valent iron (ZVI).

TEM images demonstrate that Fe⁰ was distributed in chain like manner over activated carbon (Fig. 3a). Fe⁰-AC comprised of rod like and spherical particles arranged in irregular fashion. The average size of Fe⁰-AC carbon was found to be 50 nm while ZVI particles tend to form aggregation in the range of 200 nm. TEM results clearly indicated the agglomeration of ZVI in the absence of activated carbon and were in agreement with SEM analysis.

Fig. 4a–c demonstrates EDX images of AC, ZVI and Fe⁰-AC. In Fe⁰-AC, zero valent iron (45%) and activated carbon (51%) are the main constituents of nanocomposite. XRD pattern of Fe⁰-AC shows characteristics peaks of zero valent iron at $2\theta = 44.9^\circ$ and 73.3° (Fig. 4d). The broad peak at $2\theta = 22^\circ$ confirmed the presence of activated carbon (AC) in Fe⁰-AC [35]. Crystalline size of the Fe⁰-AC was calculated using Debye-Scherer formula and found to be 50 nm. These results are in approximation with TEM analysis.

3.1.2. FTIR analysis

Table 1 depicts FTIR analysis of Fe⁰-AC, MG-loaded Fe⁰-AC and Fe⁰-AC after MG degradation. The characteristic absorption bands

of Fe-O were observed at 420 cm^{-1} and 618 cm^{-1} , which confirmed the presence of zero valent iron [36]. The band at 3393 cm^{-1} ascribed to OH stretching vibration and one at 1636 cm^{-1} to the OH bending vibration of surface-adsorbed water of AC [37]. The peaks at 2805 and 1108 cm^{-1} were due to C-H and C-O stretching vibration of activated carbon. The peak at 1384 cm^{-1} was assigned to deformation vibration of hydroxyl groups [37,38]. MG dye was successfully adsorbed onto Fe⁰-AC (Table 1). The characteristic peaks of MG loaded Fe⁰-AC are shown in Table 1.

3.1.3. pH of zero point charge (pH_{zpc})

pH_{zpc} plays very important role in adsorption process as it refers to pH at which the electrical charge density on a surface is zero. At higher pH than pH_{zpc} the surface of Fe⁰-AC and AC is negatively charged and attracts cations. Conversely, below pH_{zpc} , the surface is positively charged and repels cations [33]. Therefore, this parameter determines the potential of Fe⁰-AC to adsorb MG. In precedent study, pH_{zpc} of Fe⁰-AC and AC were 6.00 and 6.10, respectively (Fig. 5a and b).

Table 1

FTIR analysis of Fe⁰-AC, MG loaded Fe⁰-AC and Fe⁰-AC after six cycles.

Catalyst	Band (cm^{-1})	Inference	Reference
Fe ⁰ -AC	420, 618	Fe-O stretching vibrations	[36]
	2805, 1108	C-H stretching vibration and C-O stretching vibration of AC	[37]
	3393, 1636	O-H stretching and bending of vibration of H_2O	[38]
MG loaded Fe ⁰ -AC	405	C-H bending vibrations due to aromatic structure	[36]
	587	C-N stretching vibrations of aromatic structure	[38]
	850–670	C-H bending vibrations due to aromatic structure	[38]
	1156	C-H bending vibrations of asymmetric CH_3 group	[38]
	1368	C-N stretching of aromatic tertiary amine	[38]
	1478	C-H bending vibrations of asymmetric CH_3 group	[38]
	1586	C=C stretching vibration of benzene	[37]
	1640	O-H bending of vibration of H_2O	[36]
	2756	C-H stretching vibration of AC	[37]
	2917	C-H stretching of asymmetric CH_3 group	[37]
Fe ⁰ -AC after six cycles	3402	O-H stretching vibrations of AC	[37]
	415	O-H stretching vibrations of AC	[36]
	1150	C-O stretching vibration of AC	[37]
	1610	bending of vibration of H_2O	[37]
	3409	Fe-O stretching vibration	[36]

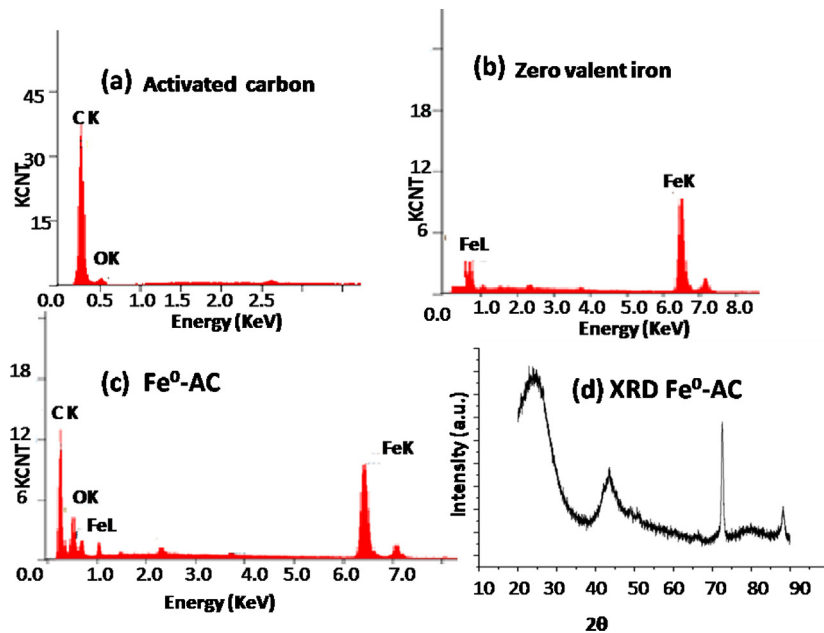


Fig. 4. EDX (a–c) and XRD (d) spectra of activated carbon, zero valent iron and $\text{Fe}^0\text{-AC}$.

UV-visible analysis was performed by dispersing AC and $\text{Fe}^0\text{-AC}$ in ethanol (Fig. 5c). The characteristic peaks of zero valent iron were observed at 200 nm and 260 nm [39].

3.2. Degradation of MG by solar/ $\text{H}_2\text{O}_2\text{/cit./Fe}^0\text{-AC}$ system at circumneutral pH

In precedent study, malachite green was selected as target organic substrate to explore photocatalytic efficiency of $\text{Fe}^0\text{-AC}$. MG was photo-stable and citrate-ferric complexes did not influence the absorption spectrum at 620 nm. The pH of solution was kept at 6.75 for solar/ $\text{H}_2\text{O}_2\text{/cit./Fe}^0\text{-AC}$ system. Fig. 6a displays the changes in the temporal absorption of spectra of MG in solar/ $\text{H}_2\text{O}_2\text{/cit./Fe}^0\text{-AC}$ system. The dye color was changed from initial blue to

nearly colorless. The main chromophoric peak at 620 nm decreased rapidly and disappeared in 60 min of radiation time. The blue-shift of 10 nm ($\Delta\lambda = 620\text{--}610\text{ nm}$) was observed during decolorization of MG. The decrease at 620 nm was due to the destruction of conjugated aromatic ring system. While blue shift from 620 to 610 nm depicted de-ethylation of MG [40]. Therefore, it can be inferred that both cleavage of chromophoric ring and de-ethylation process proceeded during MG removal. The decolorization of MG followed pseudo first order kinetics (R^2 , 0.95) with rate constant of $9 \times 10^{-2}\text{ s}^{-1}$ (Fig. 6b).

During Fe^0 and H_2O_2 mediated degradation processes, corrosive dissolution of Fe^0 is a matter of concern for the researchers [22]. The erosion of Fe^0 should be low for the efficacy of process. In case of $\text{Fe}^0\text{-AC}$, 0.9 μmol of Fe (II) was found in reaction solution after 60 min.

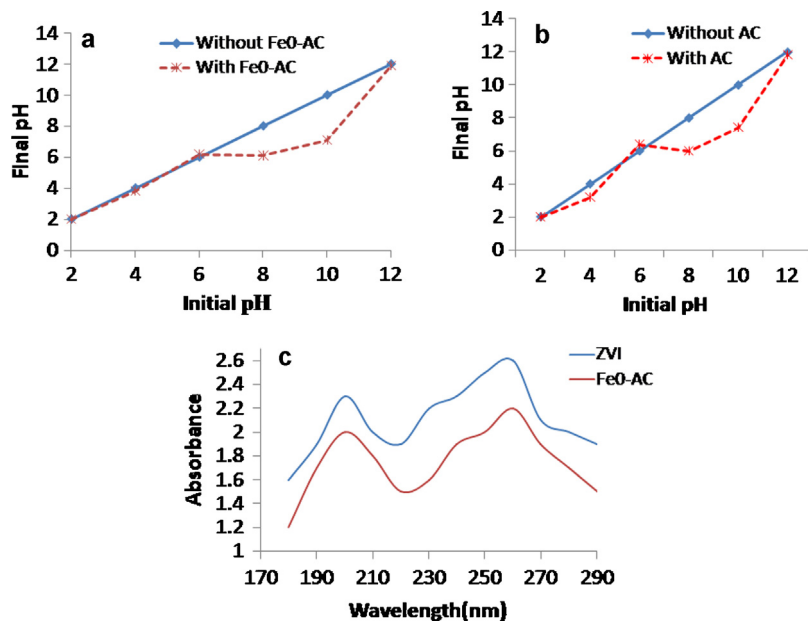


Fig. 5. (a–c) pH_{zpc} of $\text{Fe}^0\text{-AC}$ (a) and AC (b). (c) UV spectrum of ZVI and $\text{Fe}^0\text{-AC}$.

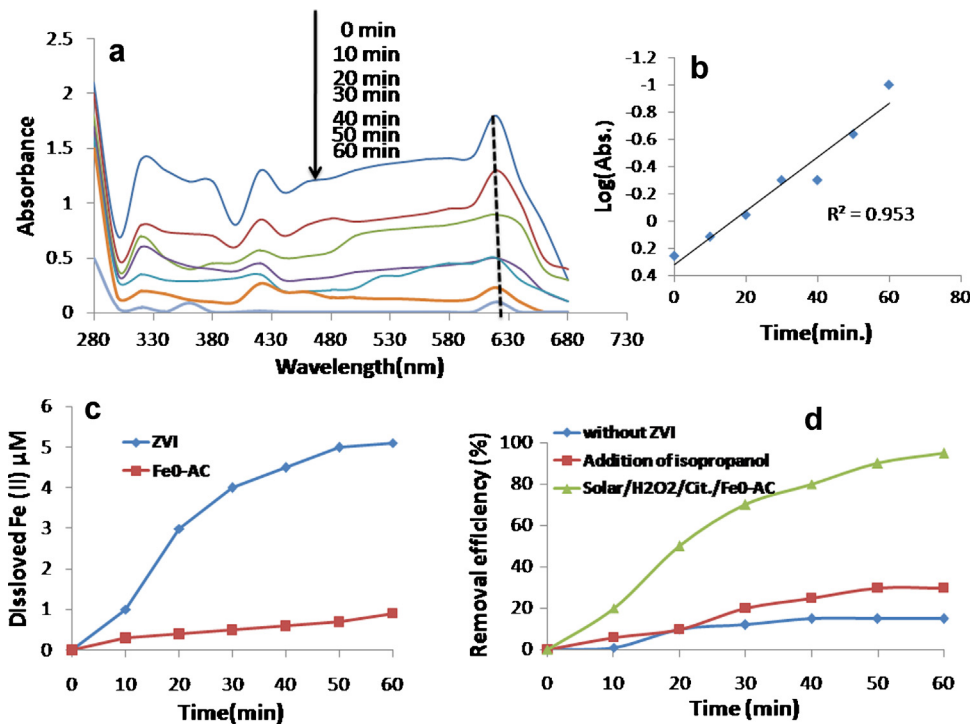


Fig. 6. (a–d) (a) UV-visible spectrum of MG degradation. (b) Log(absorbance) vs Time plot. (c) Concentration of dissolved Fe(II). (d) Effect of isopropanol on MG removal in using solar/H₂O₂/cit./Fe⁰-AC system. Reaction conditions: [MG] = 3.5 × 10⁻⁵ M, [H₂O₂] = 7.0 × 10⁻⁴ M, [cit.] = 4 × 10⁻⁵ M, catalyst dosage = 60 mg/50 mL, pH = 6.75, solar light intensity = 35 × 10³ ± 1000 lx, isopropanol = 3 × 10⁻³ M, temperature = 30 ± 0.3 °C and time = 60 min.

However, 5.0 μmol of Fe(II) was released in case of ZVI (Fig. 6c). It clearly indicated that corrosive dissolution of Fe⁰ was quite lower in Fe⁰-AC. About 15% of MG was removed in the absence of Fe⁰.

To investigate the role of OH[•] radicals in photo-degradation, experiments were performed with isopropanol. Isopropanol containing α-hydrogen is highly reactive with OH[•] where as poorly with O₂[−]. Buxton et al. has described high second order rate constant (6 × 10⁹ M^{−1} s^{−1}) of isopropanol with OH[•] radicals [41]. Fig. 6d depicts the effect of isopropanol on the degradation of MG. Only 15% of MG was removed in the presence of isopropanol due to quenching of hydroxyl radicals. These results indicated that MG degradation predominantly occurred via OH[•] radical assisted oxidative pathway.

3.3. Adsorption studies for MG removal

The adsorption of MG onto Fe⁰-AC is an important parameter for efficient dye removal. The amount of MG adsorbed per gram of adsorbent at time t (min) can be found by Eq. (7) [42,43]

$$g_t = \frac{(C_0 - C_t)V}{m} \quad (7)$$

where q_t (mmol g^{−1}) is the amount of adsorbed MG/CR per gram of adsorbent at time t (min), C_0 is the initial concentration of MG in solution (dm^{−3}), C_t is the concentration of MG (mol dm^{−3}) at time t (min), V is the volume of the solution (50 mL) and m is the mass of the adsorbent (g). The percentage of MG removal in dark k are plotted in Fig. 7a. 75% of MG was removed in 45 min using Fe⁰-AC as an adsorbent. While in case of ZVI, only 10% of MG was removed in 30 min. In the present study, adsorption data was modeled using Langmuir and Freundlich isotherms. Freundlich isotherm model is given by following equation [42,43]:

$$\ln q_e = \ln k_f + \frac{1}{n} \ln C_e \quad (8)$$

where q_e is amount of adsorbate adsorbed per unit weight of adsorbent (mg/g), stands for adsorption capacity and C_e is the initial amount of adsorbate. K_f stands for Freundlich constant and was calculated from the plot $\ln q_e$ versus $\ln C_e$ (Fig. 7b). The obtained K_f was found to be 0.25 (Table 2). Langmuir isotherm is given by Eq. (9):

$$q_e = \frac{q_0 b C_e}{1 + b C_e} \quad (9)$$

where q_e is amount of adsorbate adsorbed per unit weight of adsorbent (mg/g), q_0 is the monolayer adsorption capacity (mg/g) and b is the Langmuir constant (L/mg). Langmuir isotherms for MG adsorption onto Fe⁰-AC and ZVI plots were plotted in Fig. 7c. Langmuir isotherm model exhibited better fit to data for MG removal by Fe⁰-AC and ZVI than Freundlich isotherm. The value of q_{\max} was found to be 100 mg/g (Table 2). This suggests that monolayer adsorption occurred uniformly on the active sites of the adsorbents [42]. These results indicated that adsorption of MG was an important parameter in Fe⁰-AC based solar Fenton's reaction for efficient degradation of dye.

Table 2

Langmuir and Freundlich isotherm parameters for MG adsorption: MG concentration = 5 × 10^{−5} mol dm^{−3}, contact time = 50 min, temperature = 30 ± 1 °C and pH = 6.75.

Parameter	Fe ⁰ -AC	ZVI
<i>Langmuir</i>		
q_{\max} (mg/g)	100.12	25.5
b (L/mg)	3.56	1.2
R^2	0.985	0.984
<i>Freundlich</i>		
N	9.12	3.2
K_f	0.25	0.05
R^2	0.95	0.94

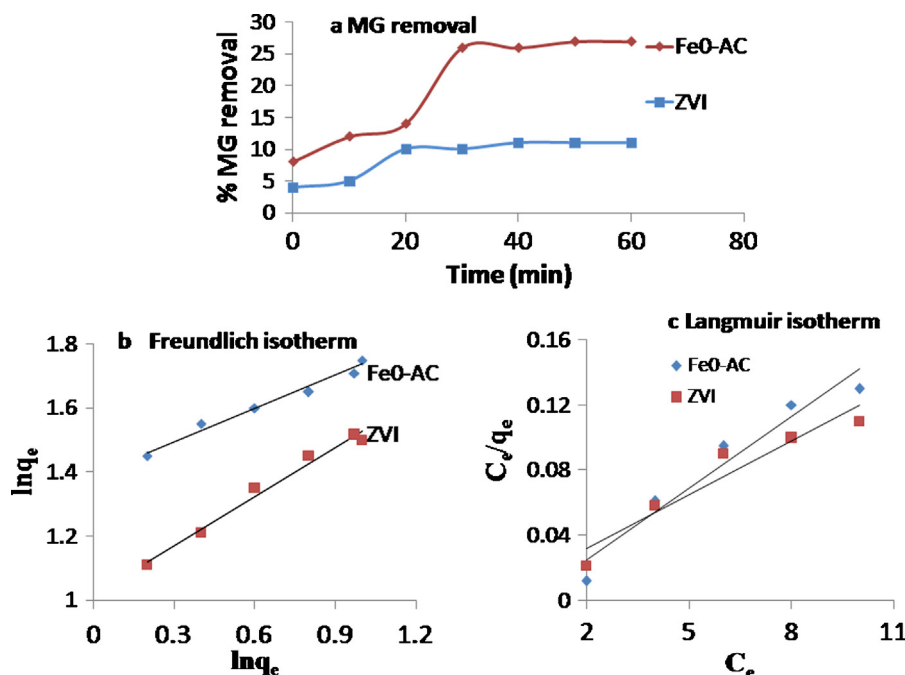
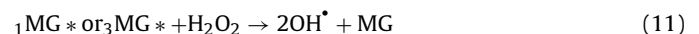


Fig. 7. Adsorption of MG onto Fe⁰-AC, ZVI: (a) Percentage removal of malachite green in dark, (b) Freundlich isotherm model for MG adsorption and (c) Langmuir isotherm model for MG adsorption. Reaction condition: [MG] = 3.5×10^{-5} M, adsorbent dosage = 60 mg/50 mL, pH = 6.75, temperature = 30 ± 0.3 °C and time = 60 min.

3.4. Control experiments for MB degradation

MG removal was explored under solar/H₂O₂/cit./Fe⁰-AC, solar/cit./Fe⁰-AC, solar/H₂O₂/Fe⁰-AC, solar/H₂O₂/cit., solar/cit./AC and solar/cit./Fe⁰ treatment systems (Fig. 8a and b). About 40% of MG was removed in both solar/H₂O₂/Fe⁰-AC and solar/cit./Fe⁰-AC systems. The MG removal efficiency followed the order: solar/H₂O₂/cit./Fe⁰-AC > solar/H₂O₂/Fe⁰-AC ≈ solar/cit./Fe⁰ ≈ solar/cit./Fe⁰-AC > solar/H₂O₂/cit./AC > solar/cit./AC (Fig. 8a). Solar/cit./H₂O₂ system was able to remove MG in the absence of F⁰-AC. It indicated that OH[·]

radicals could be produced via H₂O₂ and solar light interactions through dye sensitization process (Eqs. (10) and (11)) [44].



In solar/cit./Fe⁰-AC, 66% of MG was removed in 60 min. It shows that MG was mainly removed through reductive pathway in absence of H₂O₂ via following reactions (Eq. (12) and (13)) [45].

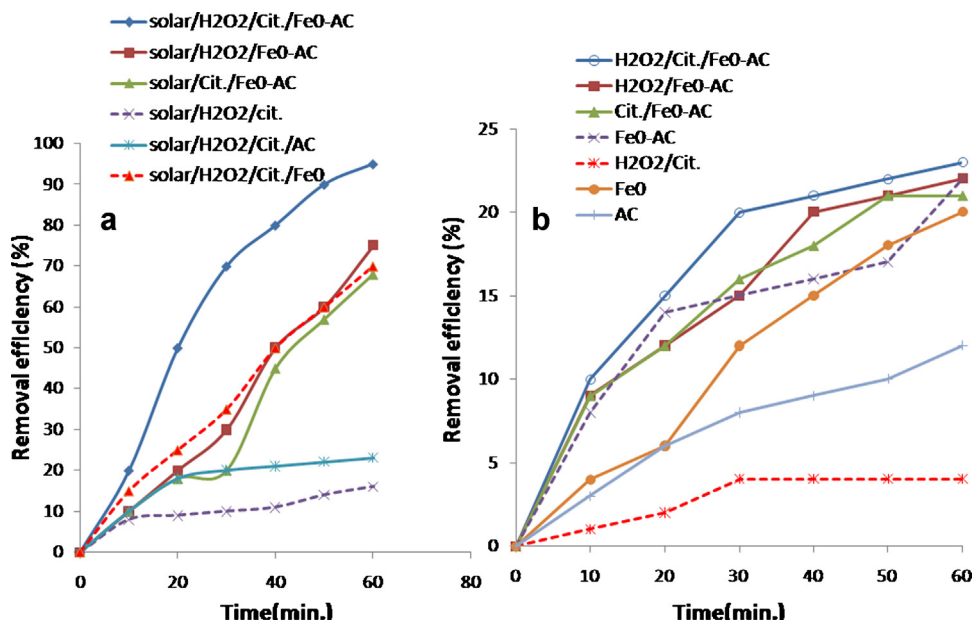


Fig. 8. (a–b) MG removal under different reaction systems (a) solar (b) in dark. Reaction condition: MG = [MG] = 3.5×10^{-5} M, [H₂O₂] = 7.0×10^{-4} M, [cit.] = 4×10^{-5} M, catalyst dosage = 60 mg/50 mL, pH = 6.75, solar light intensity = $35 \times 10^3 \pm 1000$ lx, temperature = 30 ± 0.3 °C and time = 60 min.

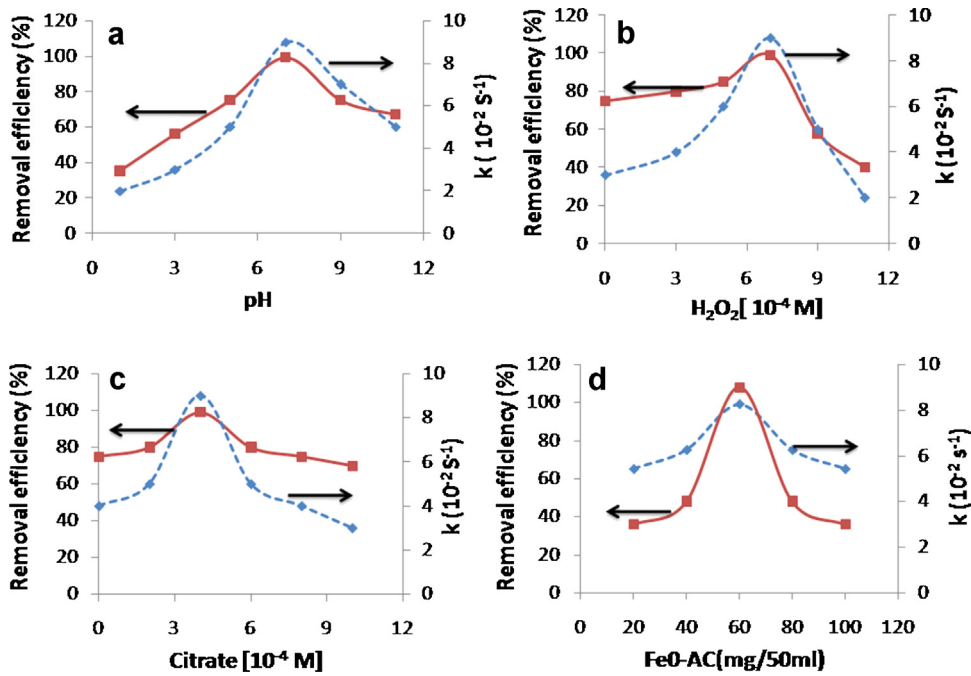
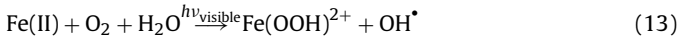


Fig. 9. (a-d) Effect reaction parameters, pH (a), H₂O₂ dosage (b), citrate dosage (c), and Fe⁰-AC (d) dosage on MG removal using solar/H₂O₂/cit./Fe⁰-AC system. Reaction conditions: [MG] = 3.5 × 10⁻⁵ M, [H₂O₂] = 7.0 × 10⁻⁴ M, [cit.] = 4 × 10⁻⁵ M, catalyst dosage = 60 mg/50 mL, pH = 6.75, solar light intensity = 35 × 10³ ± 1000 lx, temperature = 30 ± 0.3 °C and time = 60 min.



The removal experiments were also performed in the absence of solar light (Fig. 8b). The removal efficiency followed the sequence: H₂O₂/cit./Fe⁰-AC ≈ H₂O₂/Fe⁰-AC > cit./Fe⁰-AC ≈ Fe⁰-AC/Fe⁰ > Fe⁰ > AC > H₂O₂/Cit. Without irradiations, 23% of MG removal was achieved using H₂O₂/cit./Fe⁰-AC system. Very low removal efficiency was observed for AC, Fe⁰-AC and H₂O₂ treatment systems. In general, from the view point of individual factor importance, the achieved prohibitive order followed the trend: solar light > Fe⁰-AC > Fe⁰ > H₂O₂ > AC > cit.

3.5. Reaction parameter affecting solar/H₂O₂/cit./Fe⁰-AC

Since reaction pH, Fe⁰-AC, H₂O₂ and citrate concentration were the most important parameters influencing MG removal in solar/H₂O₂/cit./Fe⁰-AC system. So, all experiments were carried out individually to check extent of MG degradation.

The effect of pH on MG removal was investigated in range of 2–11 using solar/H₂O₂/cit./Fe⁰-AC system (Fig. 9a). The experimental data were fitted to pseudo first order kinetics ($R^2 = 0.97$). The MG degradation enhanced with increase in pH from 1 to 7.5. However, further increase in pH caused a reduction in rate constant. The adsorption of dye is prerequisite parameter in the effective photo degradation process. At lower pH below pH_{pzc}, positively charged surface of Fe⁰-AC was resulted in low adsorption of MG on the catalyst surface. With increase in pH above pH_{pzc}, more negatively charged surface of Fe⁰-AC resulted in higher adsorption of MG. However, excessive MG adsorption resulted in lowering of rate constant due to screening of solar light leading to reduction in photo active volume [44,46].

Fig. 9b depicts the effect of H₂O₂ concentration on MG removal in solar/H₂O₂/cit./Fe⁰-AC system. The rate constant increased from 2×10^{-2} to $9 \times 10^{-2} \text{ s}^{-1}$ with increase in H₂O₂ from 3×10^{-4} to 9×10^{-4} M. The increased rate constant was due to enhanced formation of hydroxyl radicals (OH[·]). However, further increase in H₂O₂ concentration reduced MG removal. This phenomenon might

be ascribed to OH[·] radical extinguishing, and self-decomposition of H₂O₂ due to excessive addition of H₂O₂ (Eqs. (14) and (15)) [44,47].

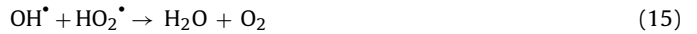
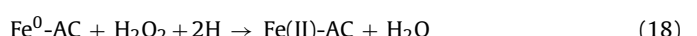
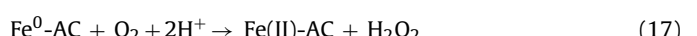


Fig. 9c shows the effect of citrate ion on MG removal in solar/H₂O₂/cit./Fe⁰-AC system. MG removal efficiency was found to increase with an increment in 2×10^{-4} to 4×10^{-4} M of citrate ion, which could be due to higher absorption of visible light by Fe(III)citrate-OH[−] complex in photoactive volume. However, further increase in citrate concentration reduced the rate reaction. This reduction was attributed to the consumption of hydroxyl radicals by excessive citrate ions form 3-hydroxy-glutrate²⁻ [45].

The effect of Fe⁰-AC dosage on MG removal was investigated in range of 20 mg/50 mL to 100 mg/50 mL (Fig. 9d). The rate constant was optimal at 60 mg/50 mL of Fe⁰-AC loading ($9 \times 10^{-2} \text{ s}^{-1}$). The increased rate constant was due to higher rate of OH[·] formation. However, further increase in Fe⁰-AC loading caused reduction in rate constant. The excessive Fe⁰-AC loading reduced the photoactive volume due to screening of solar light [44,45,67].

3.6. Proposed mechanism of MG degradation in solar/H₂O₂/citrate/Fe⁰-AC

Based on the above results and discussion, plausible mechanism for MG removal was deduced. First of all, MG was adsorbed onto surface of Fe⁰-AC in dark and surface of Fe⁰-AC became blue (Eq. (16)). After this, solution was exposed to solar light. Fe⁰ was converted into Fe(II) under aerobic condition (Eqs. (17) and (18)) also through dye sensitization process (Eq. (11)). Photo-Fenton reaction was initiated by Fe(II) and H₂O₂ to produce hydroxyl radicals(OH[·]) and Fe(III)(Eqs. (16)–(19)) [27].



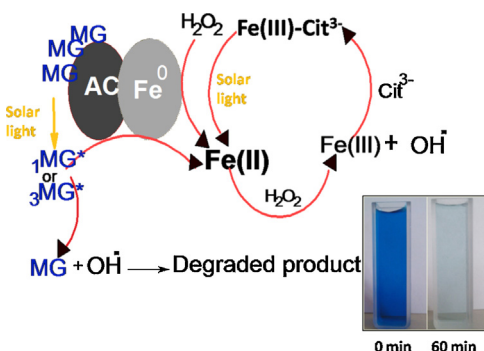
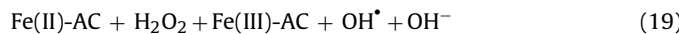
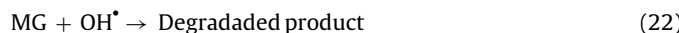


Fig. 10. Diagrammatic representation of proposed mechanism for MG degradation from aqueous phase using solar/ H_2O_2 /cit./ Fe^0 -AC system. Inset is MG under solar/ H_2O_2 /cit./ Fe^0 -AC system at 0 min and 60 min. Reaction conditions: $[MG] = 3.5 \times 10^{-5}$ M, $[H_2O_2] = 7.0 \times 10^{-4}$ M, $[cit.] = 4 \times 10^{-5}$ M, catalyst dosage = 60 mg/50 mL, pH = 6.75, solar light intensity = $35 \times 10^3 \pm 1000$ lx, temperature = 30 ± 0.3 °C and time = 60 min.



The formation of $Fe(III)$ citrate- OH^- complex with $Fe(III)$ ions could be attributed to the citrate. $Fe(III)$ citrate- OH^- complex transformed into $Fe(II)$ and citrate- OH^\bullet through visible light absorption. The produced $Fe(II)$ could participate in OH^\bullet formation (Eq. (20)–(22)) [27].



The citrate ions were converted into 3-hydroxo-glutrate $^{2-}$ leading to the formation of acetone and CO_2 [27]. The introduction of solar light could largely enhance the generation of Fe^{2+} , ultimately leading to enhanced formation of hydroxyl radicals. Finally, OH^\bullet radical degraded MG dye and catalyst was recovered to its original position (Fig. 10).

3.7. The repeatability of Fe^0 -AC and ZVI

The recycle efficiency of Fe^0 -AC and ZVI was explored under solar/ H_2O_2 /cit. system. The separation of Fe^0 -AC was quick and easy due to low agglomeration. However, separation of ZVI was slow and complicated. The efficiency of ZVI was reduced to 12% after 6

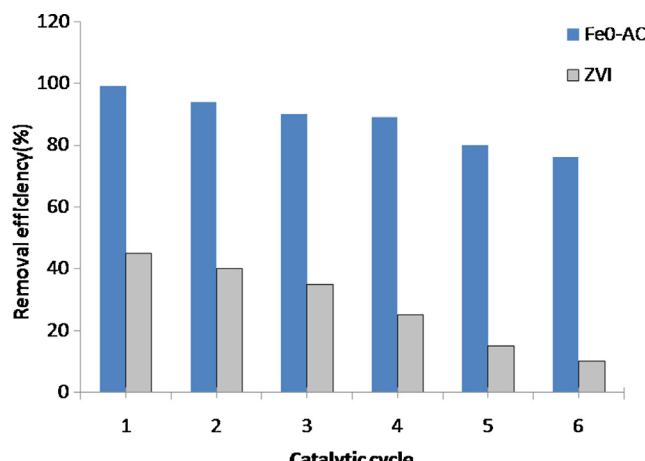


Fig. 11. Recycle efficiency of Fe^0 -AC and ZVI. Reaction conditions: $[MG] = 3.5 \times 10^{-5}$ M, $[H_2O_2] = 7.0 \times 10^{-4}$ M, $[cit.] = 4 \times 10^{-5}$ M, catalyst dosage = 60 mg/50 mL, pH = 6.75, solar light intensity = $35 \times 10^3 \pm 1000$ lx, temperature = 30 ± 0.3 °C and time = 60 min.

catalytic cycles (Fig. 11). On the other hand, no significant changes in FTIR spectrum of Fe^0 -AC were recorded after 6 cycles (Table 1) Fe^0 -AC was easily reused with 75% efficiency for six cycles.

4. Conclusion

A new solar/ H_2O_2 /cit./ Fe^0 -AC system was developed for the removal of MG at circum neutral pH. It showed high removal efficiency for dye removal. MG was completely decolorized in 60 min of reaction time. Control test and factor experiments indicated that MG removal mainly occurred through OH^\bullet radicals. The removal of MG was higher at circumneutral pH 6.75, which was quite different from Fenton reaction. Hydroxyl radical formation was largely enhanced by the citrate ions and solar light. Fe^0 -AC had higher recycle efficiency compared to ZVI. The enhanced oxidative treatment is the main advantage of investigated system. Solar/ H_2O_2 /cit./ Fe^0 -AC system would provide an alternative for tedious dye removal treatment.

References

- J. Cao, B.D. Luo, H.L. Lin, B.Y. Xu, S.F. Chen, Appl. Catal. B 111–112 (2012) 288–296.
- M.G. Antoniou, A.A. de la Cruz, D.D. Environ. Sci. Technol. 44 (19) (2010) 7238–7244.
- H. Hassan, B.H. Hameed, Chem. Eng. J. 171 (2011) 912–918.
- Y. Sun, J.J. Pignatello, Environ. Sci. Technol. 27 (1993) 304–310.
- O. Rozas, D. Contreras, M.A. Mondaca, M. Perez-Moya, H.D. Mansilla, J. Hazard. Mater. 177 (2010) 1025–1030.
- J.Y. Feng, X.J. Hu, P.L. Yue, S.Z. Qiao, Sep. Purif. Technol. 67 (2009) 213–217.
- Z.H. Ai, L.R. Lu, J.P. Li, L.Z. Zhang, J.R. Qiu, M.H. Wu, J. Phys. Chem. C 111 (2007) 7430–7436.
- A. Noopur, J. Sharma, S. Sharma, S. Kumar, P.B. Punjabi, Ind. J. Chem. A 51A (2012) 943–948.
- A.L.T. Pham, C. Lee, F.M. Doyle, D.L. Sedlak, Environ. Sci. Technol. 43 (2009) 8930–8935.
- H.W. Ji, W.J. Song, C.C. Chen, H. Yuan, W.H. Ma, J.C. Zhao, Environ. Sci. Technol. 41 (2007) 5103–5107.
- C. Catrinescu, C. Teodosiu, M. Macoveanu, J. Miehe-Brendle, R. Le Dred, Water Res. 37 (2003) 1154–1160.
- J.E. Min, M. Kim, J.H. Pardue, J.W. Park, J. Environ. Sci. Health A43 (2) (2008) 144–153.
- X.Q. Li, D.W. Elliott, W.X. Zhang, Crit. Rev. Solid State Mater. Sci. 31 (4) (2006) 111–122.
- A. Ghauch, A. Tuqan, H.A. Assi, Environ. Pollut. 157 (2009) 1626–1635.
- Z. Fang, J. Chen, X. Qiu, W. Cheng, L. Zhu, Desalination 268 (2011) 60–67.
- J. Fan, Y. Guo, J. Wang, M. Fan, J. Hazard. Mater. 166 (2009) 904–910.
- H.L. Lien, W.X. Zhang, J. Environ. Eng. 125 (1999) 1042–1047.
- D.W. Elliott, H.L. Lien, W.X. Zhang, J. Environ. Eng. 135 (2009) 317–325.
- R.D. Ambashta, E. Repo, M. Sillanpaa, Ind. Eng. Chem. Res. 50 (2011) 11771–11777.
- X. Zhang, Y.M. Lin, X.Q. Shan, Z.L. Chen, Chem. Eng. J. 158 (2010) 566–570.
- R. Cheng, J.L. Wang, W.X. Zhang, J. Hazard. Mater. 144 (2007) 334–339.
- B. Schrick, B.W. Hydutsky, J.L. Blough, T.E. Mallouk, Chem. Mater. 16 (2004) 2187–2193.
- J. Xu, N. Gao, Y. Deng, S. Xia, Chem. Eng. J. 222 (2013) 520–526.
- K. Selvam, M. Muruganandham, M. Swaminathan, Sol. Energy Mater. Sol. Cells 89 (2005) 61–74.
- J. Lee, J. Kim, W. Choi, Environ. Sci. Technol. 41 (2007) 3335–3340.
- V.A. Nadtochenko, J. Kiwi, Inorg. Chem. 37 (1998) 5233–5238.
- H. Katsumata, S. Kaneko, T. Suzuki, K. Ohta, Y. Yobiko, J. Photochem. Photobiol. A 180 (2006) 38–45.
- M.R.A. Silva, A.G. Trovo, R.F.P. Nogueira, J. Photochem. Photobiol. A 191 (2007) 187–192.
- M.S. Lucas, J.A. Peres, Dyes Pigments 74 (2007) 622–629.
- J. Guo, Y. Du, Y. Lan, J. Mao, J. Hazard Mater. 186 (2011) 2083–2088.
- L.N. Shi, X. Zhang, Z.L. Chen, Water Res. 45 (2011) 886–892.
- W.B. Fortune, M.G. Mellon, Ind. Eng. Chem. 10 (1938) 60–64.
- S. Yadav, V. Srivastava, S. Banerjee, C.H. Weng, Y.C. Sharma, Catena 100 (2013) 120–127.
- Z. Al-Qodah, R. Shawabkah, Braz. J. Chem. Eng. 26 (1) (2009) 127–136.
- Z.X. Chen, X.Y. Jin, Z. Chen, M. Megharaj, R. Naidu, J. Colloid. Interface Sci. 363 (2011) 601–607.
- G. Socrates, Infrared Characteristic Group Frequencies, John Wiley and Sons, Ltd., New York, 1980, pp. 145.
- J. Coates, in: R.A. Meyers (Ed.), A Practical Approach in Encyclopedia of Analytical Chemistry, John Wiley & Sons, Chichester, UK, 2000, pp. 10815–10837.

- [38] J.M. Dyer, Application of Absorption Spectroscopy of Organic Compounds, Prentice Hall of India Private Limited, 2005, pp. 33–38.
- [39] Y. Kumar, V. Elango, V. Rajendran, N. Kannan, *Dig. J. Nanomater. Bios.* 6 (4) (2011) 1771–1776.
- [40] G. Guandao, Z. Aiyong, Z. Meng, C. Jinlong, Z. Quanxing, *Chin. J. Catal.* 29 (5) (2008) 426–430.
- [41] G.V. Buxton, C. Greenstock, W.P. Hellman, A.B. Ross, *J. Phys. Chem.* 17 (1988) 513–886.
- [42] V.K. Gupta, D. Pathania, S. Sharma, P. Singh, *J. Colloid Interface Sci.* 401 (2013) 125–132.
- [43] A. Khaled, A. El-Nemr, A. El-Sikaily, O. Abdelwahab, *Desalination* 238 (2009) 210–232.
- [44] I.K. Konstantinou, T.A. Albanis, *Appl. Catal. B* 499 (1) (2004) 1–14.
- [45] S.A. Kim, S. Kamala-Kannan, K.J. Lee, Y.J. Park, P.J. Shea, W.H. Lee, H.M. Kim, B.T. Oha, *Chem. Eng. J.* 217 (2013) 54–60.
- [46] V.K. Gupta, D. Pathania, S. Agarwal, P. Singh, *J. Hazard Mater.* 243 (2012) 179–1862.
- [47] B. Pare, S.B. Jonnalagadda, H. Tomar, P. Singh, V.W. Bhagwat, *Desalination* 232 (2008) 80–90.